Magnetic Cytoskeleton Affinity Purification of Microtubule Motors Conjugated to Quantum Dots

Marco Tjioe,[†,‡,§] Hyeon Ryoo,[‡,‖] Yuji Ishitsuka,[‡,§] Pinghua Ge,[‡,§] Carol Bookwalter,[‖] Walter Huynh,[#] Richard J. McKenney,[¶] Kathleen M. Trybus,[⊥] and Paul R. Selvin*,[†,‡,§]

[†]Center for Biophysics and Computational Biology, [‡]Center for the Physics of Living Cells, and [§]Department of Physics, [‖]Bioengineering and Biomedical Engineering, University of Illinois at Urbana−Champaign, Urbana, Illinois 61801, United States

[⊥]Department of Molecular Physiology and Biophysics, University of Vermont, Burlington, Vermont 05405, United States

[#]Department of Cellular and Molecular Pharmacology, University of California, San Francisco, San Francisco, California 94143, United States

[¶]Molecular & Cellular Biology, University of California, Davis, La Jolla, California 92093, United States

S *Supporting Information*

ABSTRACT: We develop magnetic cytoskeleton affinity (MiCA) purification, which allows for rapid isolation of molecular motors conjugated to large multivalent quantum dots, in miniscule quantities, which is especially useful for single-molecule applications. When purifying labeled molecular motors, an excess of fluorophores or labels is usually used. However, large labels tend to sediment during the centrifugation step of microtubule affinity purification, a traditionally powerful technique for motor purification. This is solved with MiCA, and purification time is cut from 2 h to 20 min, a significant time-savings when it needs to be done daily. For kinesin, MiCA works with as little as

0.6 μg protein, with yield of ~27%, compared to 41% with traditional purification. We show the utility of MiCA purification in a force-gliding assay with kinesin, allowing, for the first time, simultaneous determination of whether the force from each motor in a multiple-motor system drives or hinders microtubule movement. Furthermore, we demonstrate rapid purification of just 30 ng dynein-dynactin-BICD2N-QD (DDB-QD), ordinarily a difficult protein-complex to purify.
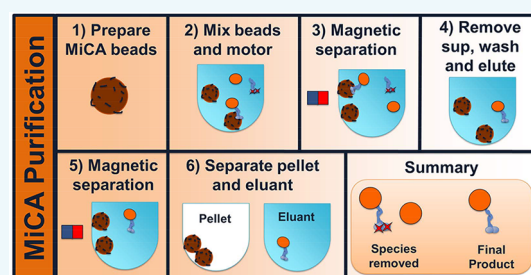
INTRODUCTION

Kinesin, dynein, and myosin are cytoskeletal motor proteins that convert chemical energy into mechanical work to power most of the movements within the cell. They are responsible for a wide range of motion inside the cell from membrane trafficking to movement of the entire cell.[1] Their defects are implicated in many diseases.[2−11]

Single molecule studies offer powerful means to uncover mechanisms of motor movements, allowing examination of the step-sizes[12−20] and forces[17,19,21−25] generated by a single motor. A recurring challenge in single molecule studies is ensuring that measurements are done on one motor. This is challenging with large labels as they tend to be multivalent, and thus can attach to multiple motors. A common solution is to mix excess labels per motor,[26−32] but this procedure contributes to noise and increase unproductive events, adversely affecting single molecule analysis.

To remove excess labels and obtain active microtubule-based motors, many laboratories use the well-established microtubule affinity purification.[33−37] In this method, motors bind to and are subsequently released from microtubules with the addition of ATP, while excess labels remain unbound and are washed away after centrifugation. It has been applied to purify unlabeled motors from cellular extract,[34,38] and motors

bound to fluorescent proteins[39] and organic fluorophores.[14,33] It is, however, unable to purify motors labeled with large labels, as excess labels sediment during the high speed centrifugation, preventing their separation from labeled motors. To the best of our knowledge, no purification has been done on motors labeled to reporters larger than 10 nm, even though a significant number of studies have made use of large reporters—especially quantum dots (QD),[26−28,30−32,40,41] due to quantum dot brightness and photostability.

The other drawbacks of microtubule affinity purification include the use of a large quantity of samples (μg to mg) and long purification time (a few hours). These are not optimal for single molecule study, since only a small amount of sample is needed for each experiment, and conjugated motors may have a short lifetime before dissociating or becoming inactive.

To address these drawbacks, we developed Magnetic Cytoskeleton Affinity (MiCA) purification, which uses magnetic separation technology,[42,43] instead of a centrifugation step (Figure 1). In short, microtubules are immobilized on magnetic beads, and then labeled motors bind to, and release
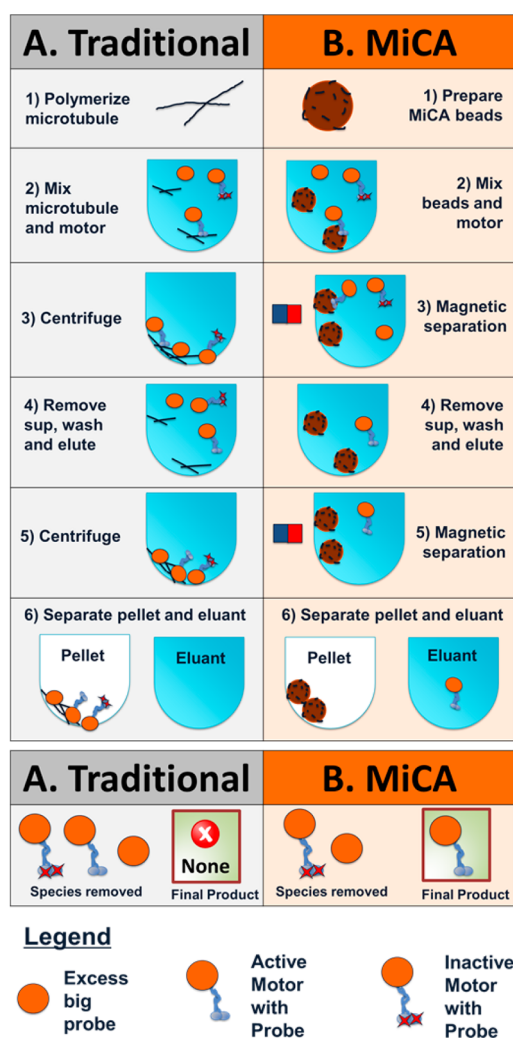
Figure 1. Comparison between (A) traditional microtubule affinity and (B) MiCA purification for isolation of motors bound to big probe. The magnetic separation (steps 3 and 5) for MiCA purification replaces centrifugation used in traditional purification. MiCA purification enables separation of active motors attached to large probes from inactive motors and excess probes, which is not possible with traditional purification.

from, the immobilized microtubules using different ATP analogues. The result is isolated motors labeled with quantum dots, free of any unlabeled quantum dots and inactive motors incapable of binding microtubules. The key to a robust MiCA purification is to use moderately positive magnetic beads with long PEG chain, as shown in Figure 2. This works well as the positively charged bead binds strongly to negatively charged microtubules, while the PEG chain effectively prevents nonspecific interaction with motors, allowing motors to bind and release.

Here we demonstrate the efficacy of MiCA purification on kinesin bound to QD, on kinesin-only for comparison with traditional microtubule affinity purification, and on dynein-dynactin-BICD2N (DDB) complex bound to QD. It takes only 20 min to complete MiCA purification, a significant time savings from the 2 h needed for microtubule affinity purification. The yield for MiCA purification is ∼27%, and we have successfully purified active kinesin-QD and DDB-QD in minute quantities, 640 ng and 30 ng, respectively. Finally, we demonstrate an application for purified kinesin-QD using

force-gliding assay, where, for the first time, the forces of multiple kinesin can be detected simultaneously.

■ RESULTS AND DISCUSSION

MiCA Purification Protocol. MiCA purification is derived from the traditional microtubule affinity purification. The experimental protocols for both are illustrated in Figure 1, highlighting how MiCA purification can be used to separate motors labeled with large fluorophore from inactive and excess fluorophores, while traditional purification cannot. A detailed protocol for traditional microtubule affinity purification can be found in Supporting Information section 2. The magnetic separation (steps 3 and 5) for MiCA purification replaces centrifugation used in traditional purification. Below are the six steps of MiCA purification:

1. MiCA capture beads are formed by mixing short microtubules with moderately positive magnetic beads:

- Short microtubules (<1 μm) are polymerized from 5 mg/mL tubulin at 37 °C for 30 min in the presence of 2 mM GMPCPP (nonhydrolyzable analog of GTP), then sonicated for 3 min.
- Long microtubules can also be used for MiCA purification, but short ones are preferable to allow long-term storage and prevent aggregation of motors, as discussed in Supporting Information section 1.

2. MiCA capture beads are mixed with the motor sample in the presence of 1 mM AMP-PNP:

- Three different species are illustrated in Figure 1: excess big probe, probe-bound active kinesin, and probe-bound inactive kinesin. MiCA purification removes the excess big probe and probe-bound inactive kinesin.

3. MiCA capture beads are pulled by a magnet positioned outside of reaction tube, leaving excess big probe and probe-bound inactive kinesin in the supernatant.

4. The supernatant is removed, and the pellet is washed with dilution buffer 2−3 times, and then eluted with 1−3 mM ATP, which releases probe-bound active kinesin from MiCA capture beads.

5. MiCA capture beads are again pulled by magnet, leaving probe-bound active kinesin in the supernatant.

6. The supernatant is transferred to a new centrifuge tube separate from the pellet.

Magnetic Bead Preparation. An important element to the robustness of MiCA purification is the magnetic beads used to bind microtubules. We use charge interaction to couple positively charged amine beads to the negatively charged microtubules. However, we find that commercial amine beads are too positively charged: they will bind strongly not only to microtubule but also to kinesin, preventing kinesin from being eluted. We therefore reduce the positive charge on the beads by coupling PEG-amine, resulting in moderately positive beads that bind to microtubule, but not kinesin. The synthesis of this PEG-amine bead is illustrated in Figure 2A, with detailed protocol outlined in Supporting Information section 3.1. Briefly, commercial amine beads are washed with double-distilled water (ddH$_2$O), and then reacted with FMOC-NH-PEG-SVA (Laysan Bio, Inc.). The reaction yields FMOC-coated beads, which is washed with ddH$_2$O. The FMOC beads are then deprotected with piperidine,[44] yielding amine (NH$_2$) in place of FMOC-NH group, generating PEG-amine bead. These beads can be stored at 4 °C and are good for at least six months.
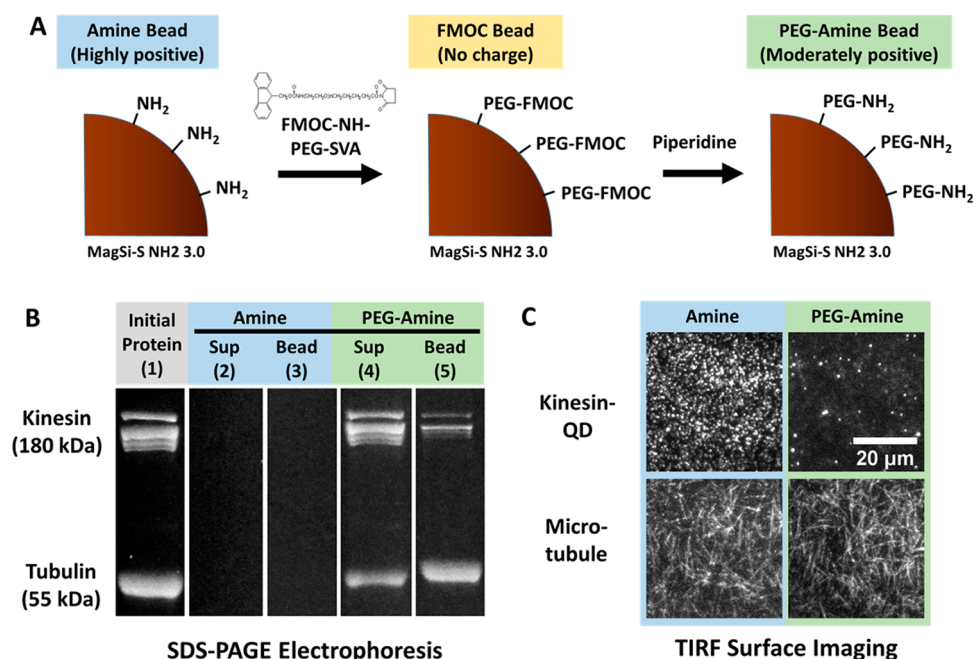
Figure 2. (A) Synthesis of PEG-amine magnetic bead from commercial amine magnetic bead. For MiCA purification to work, the bead should bind strongly to microtubules, but not to kinesin, a property that PEGylated amine-beads have, but not amine-beads. PEGylation is done by reacting commercial 3.0 μm amine bead (MagSi NH2 3.0 from Amsbio LLC) with FMOC-PEG3400-SVA (Laysan Bio, Inc.) to form PEG-FMOC bead. The FMOC group is then deprotected with piperidine to yield PEG-Amine bead. (B) To show that the PEG-amine beads bind to microtubules but not kinesin, we mix the beads with microtubules or kinesin and monitor their binding to the beads through SDS-PAGE electrophoresis. The gel image shows the initial amount of kinesin and tubulin before mixing with beads (lane 1), the amount left in the supernatant after mixing (lane 2 or 4), and the amount released from the bead after mixing with SDS detergent and incubated at 95 °C (lane 3 or 5). Amine beads bind very strongly to kinesin and microtubules so that no protein is left in the supernatant shown in lane 2 and no protein is released from bead shown in lane 3. PEG-amine beads preferentially binds to microtubules but not kinesin, shown in lane 5 where a small fraction of kinesin and a large amount of microtubules bind to the bead, and lane 4 showing that the majority of kinesin and a small fraction of microtubules are left in the supernatant after binding to PEG-amine bead. (C) TIRF surface imaging of kinesin-QD and fluorescent microtubules binding to amine and PEG-amine functionalized on glass coverslip surface. Both surfaces bind to microtubules equally well, but the amine surface binds much more to the kinesin-QD than the PEG-amine surface.

Figure 2B summarizes the result of an SDS-PAGE electrophoresis binding experiment, showing that amine beads bind strongly to both kinesin and microtubules, while PEG-amine beads bind preferentially to microtubules but not kinesin. Detailed experimental protocol is described in Supporting Information section 3.2. Briefly, kinesin and microtubules are separately mixed with amine or PEG-amine beads, and the proteins left in the supernatant (Sup) or stuck on the final beads (Bead) are monitored. The binding of kinesin and microtubules to amine beads is so strong that no protein is detected in the supernatant shown in lane 2 and no protein is released from beads shown in lane 3 even after mixing with SDS detergent and heating to 95 °C. With PEG-amine beads, kinesin binding is minimized, as a significant amount of kinesin remains in the supernatant shown in lane 4, and only a small fraction then sticks to PEG-amine beads shown in lane 5. PEG-amine beads still preserve its ability to bind microtubules, as only a small fraction of microtubules remain in the supernatant shown in lane 4, but a large fraction sticks to PEG-amine beads shown in lane 5. We perform a control experiment using BSA to block amine and PEG-amine beads, and the result is the same for the PEG-amine beads. This result is summarized in Figure S1.

Figure 2C shows total internal reflection fluorescence (TIRF) imaging of kinesin-QD and fluorescent microtubules binding to amine and PEG-amine surfaces, providing further support that amine surfaces bind strongly to both kinesin-QD and microtubules, but PEG-amine surfaces bind only to microtubules. The detailed experiment is outlined in Supporting Information section 3.3. Control experiment summarized in Figure S2 shows that as PEG-amine concentration on the surface is reduced, fewer microtubules bind, confirming that binding of the microtubules to the surface is through the presence of PEG-amine. Another control experiment shown in Figure S3 and Movie S3 concludes that kinesin-QD moves well on microtubules adhered to the PEG-amine surface (around 70% are motile) but not on amine surface (only around 26% are motile).

Attempts to generate MiCA capture beads using other conjugation schemes failed and are discussed in Supporting Information section 3.3. In general, a good MiCA capture bead should bind strongly to microtubules, but not the motors being purified. The first experiment to run is therefore binding tests for microtubules and motors to the magnetic beads.

MiCA Reduces Purification Time 7-fold. Figure 3A summarizes the time needed for traditional affinity vs MiCA purification. Total purification time reduces from 130 min for traditional affinity to 19 min for MiCA purification. The initial microtubule polymerization and centrifugation step that takes 60 min in traditional affinity is replaced with a 5 min MiCA capture bead preparation using short microtubules stored at −80 °C. The binding and elution step takes the same time for both traditional affinity and MiCA purification, but the wash and eluant extraction are 15 times faster for MiCA than for
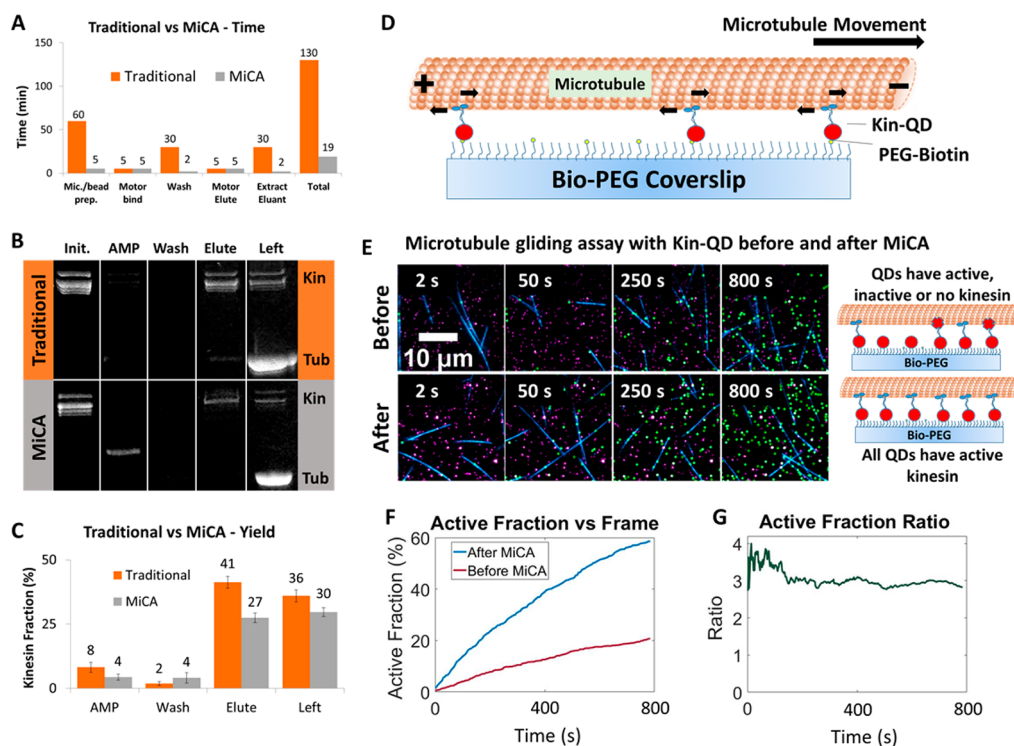
Figure 3. (A) Purification time comparison between traditional affinity vs MiCA purification. MiCA purification allows seven times reduction in total preparation time, from 130 to 19 min. (B,C) Yield comparison between traditional affinity and MiCA purification. The quantity of kinesin at each bind (AMP), wash, elute, and leftover phase is tracked. A very small amount of kinesin is seen in the bind and wash phase, showing that kinesin is efficiently bound to microtubules/MiCA capture beads. Kinesin yield with MiCA (27% in elute) is 1.5× less than that for traditional affinity purification (41%). The error bars represent standard error of the mean (standard deviation divided by square-root of sample size) obtained from gel results of 2−5 experiments. (D) Schematic diagram for microtubule gliding assay. Kinesin-streptavidin-QDs purified using MiCA attach to biotin-PEG coverslip. Imaging buffer containing microtubules and ATP is then flowed in, and microtubules will glide on top and are driven by kinesin. Kinesin walks toward the plus end of the microtubule (left) while microtubules move in the opposite direction (right). (E) Raw data showing microtubules gliding over kinesin-QD at 2, 50, 250, and 800 s before and after MiCA purification, with schematic diagram shown on right. Before MiCA purification, ∼40% QDs have no kinesin and some kinesin-QDs are inactive. These QDs will not be able to move microtubules. QD fluorescence is shown in magenta and microtubule in blue. QDs with active kinesin with prior microtubule contact are marked with green. Over time, more QDs with active kinesin contacted microtubules and are marked green. (F) Fraction of QDs with active kinesin before and after MiCA. At the end of experiment, as many as 60% of QDs after MiCA are active, compared to ∼20% before MiCA. Across all time periods, the fraction of QDs with active kinesin after MiCA is ∼3 times higher than before MiCA, as shown in panel (G).

traditional affinity purification. This is because the 30 min centrifugation time in traditional affinity is replaced with a 2 min magnetic separation in MiCA purification. Note that the 60 min initial polymerization and centrifugation step for traditional affinity protocol can be shortened to 30 min by doing batch polymerization, aliquoting and storing at −80 °C, and then start only from 30 min centrifugation to remove short microtubules, as outlined in Supporting Information section 2. This will reduce the traditional affinity purification time from 130 to 100 min, which is five times longer than that of MiCA purification.

MiCA Delivers 27% Kinesin Yield. Figure 3B,C shows traditional affinity and MiCA purification experiments monitored through SDS gel electrophoresis. Detailed protocol for this experiment can be found in Materials and Methods. The yield for each is shown in the elute lane. The yield for MiCA is 27%, 1.5× less than that of traditional affinity purification, which is 41%. The initial protein amount is shown in the first lane. This initial kinesin binds to the microtubules (for traditional) or magnetic bead (for MiCA) by the addition of AMP-PNP. The second lane (AMP) shows the amount of protein left in the supernatant and not binding to the microtubules or magnetic beads. Most kinesin binds to the

microtubules or magnetic beads. Only 8% and 4% of kinesin is left in the supernatant for traditional affinity and MiCA purification. After the binding step, the kinesin-bound microtubules or magnetic beads are washed. The wash lane shows that minimal protein is lost (2% and 4%) at this step. Once washed, the kinesin is eluted with ATP, and both the amount eluted and the amount left in beads are monitored in the Elute and Left lanes. The amounts eluted (41% and 27%) are comparable to the amounts left on microtubules or magnetic beads (36% and 30%). A second elution step can be added to increase the final yield if desired.

MiCA Allows Single Molecule Observation of Kinesin-QD in a Microtubule Gliding Assay through Removal of Free Dyes. Microtubule gliding assays generally have unlabeled kinesin bound to the surface-moving microtubules. Current effort to visualize kinesin in a gliding assay is limited to "spiking" experiments, where a high concentration of unlabeled kinesin is laid down and spiked with a low concentration of GFP-labeled kinesin.[45] These experiments suffer from the low photostability of GFP and the inability to track all the kinesin on the surface. With MiCA purification of kinesin-QD, all kinesin-QD can now be tracked, and for a very long time owing to the photostability of the QDs.
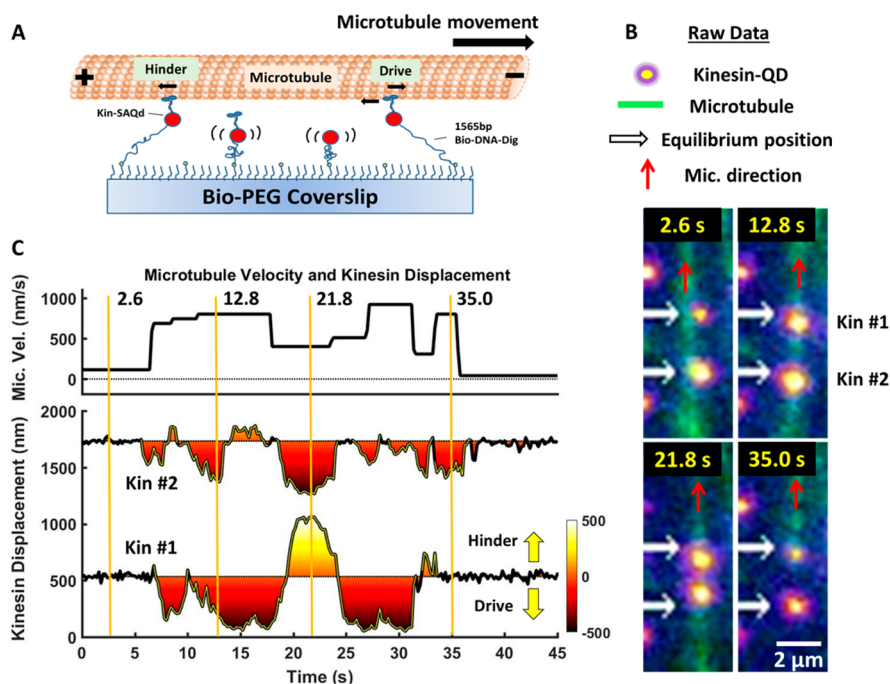
Figure 4. MiCA purification enables force-gliding assay for parallel detection of forces from multiple kinesin. (A) Schematic diagram of force gliding assay. Kinesin-QD purified with MiCA is attached to the biotin-PEG coverslip through 1565 base-pair DNA. DNA acts as a spring that allows force detection of kinesin-QD as it drives or hinders movement of the microtubules. Driving kinesin moves in the opposite direction of the microtubule, while hindering kinesin moves in the same direction. (B) Snippets of force-gliding assay at 2.6, 12.8, 21.8, and 35.0 s taken from Movie S4. Two kinesins move microtubule (green). White arrows show equilibrium kinesin positions. Red arrow shows the direction of microtubule movement. (C) Plots showing microtubule velocity and kinesin positions over time. Time points at 2.6, 12.8, 21.8, and 35.0 s corresponding to the images in (B) are marked with yellow vertical lines. At 2.6 s, microtubule velocity is ∼0 nm/s and no kinesin is attached. At 12.8 s, microtubule velocity increases to 800 nm/s when both kinesins are driving (downward displacement from equilibrium). At 21.8 s, the top kinesin remains driving, while the bottom kinesin hinders microtubules, causing the microtubule velocity to fall to 400 nm/s. At 35.0 s, the microtubule glides past the bottom kinesin, and the top kinesin becomes the sole driver, moving microtubules at 800 nm/s.

Figure 3D−G shows microtubule gliding experiments using kinesin-QD before and after MiCA purification. This is also shown in Movie S1. Detailed protocol for this experiment can be found in Materials and Methods. Figure 3E shows the fluorescence of QD (magenta) and microtubules (blue) overlaid with green dots to mark the location of QDs with active kinesin. QDs are considered active if they colocalize with microtubules for at least 8 frames (16 s). Kinesin is mixed with QD in 1:1.1 ratio. At this ratio, some QDs (∼23%) will have two or more kinesins bound, but since they will be present before and after MiCA purification, it is not critical for all QDs to be singly labeled with kinesin for this experiment. Before MiCA purification, free QDs (statistically ∼40%) and QDs with inactive kinesin are not removed. Figure 3F shows that at the end of the gliding experiment, only 20% of QDs before MiCA purification are actively gliding microtubules, compared to 60% after MiCA purification. Figure 3G shows that at any period of time the fraction of QDs with active kinesin after MiCA are approximately 3 times higher than before MiCA.

MiCA Enables Force-Gliding Assay for Parallel Detection of Forces from Multiple Kinesin. Here we show a proof-of-principle of force-gliding assay made possible by MiCA purification. This assay allows simultaneous detection of forces from multiple kinesin for the first time. The experimental setup is similar to the microtubule gliding assay with kinesin-QD shown in Figure 3D, with the addition of a 1565 base-pair double-stranded DNA between the kinesin-QD and the biotin-PEG coverslip, as shown in Figure 4A. The DNA acts as a spring that allows force detection of kinesin-QD

as it drives or hinders microtubules. Driving kinesin moves in the opposite direction of microtubule, while hindering kinesin moves in the same direction. Detailed protocol for this experiment can be found in Materials and Methods. Our current setup allows accurate detection of the direction but not the magnitude of the force exerted by kinesin on the microtubules (see Supporting Information section 16 for discussion on force accuracy).

Figure 4B shows snippets of force-gliding assay from Movie S4 at 2.6, 12.8, 21.8, and 35.0 s. Two kinesins move microtubules (green). White arrows show equilibrium kinesin positions. Red arrow shows the direction of microtubule movement. As the microtubule glides over kinesin, the two kinesin are seen driving or hindering microtubules at different times.

Figure 4C shows plots of microtubule velocity and kinesin positions over time. Time points at 2.6, 12.8, 21.8, and 35.0 s corresponding to the images in Figure 4B are marked with a yellow vertical line. At 2.6 s, microtubule velocity is ∼0 nm/s and no kinesin is attached. At 12.8 s, microtubule velocity increases to 800 nm/s when both kinesins are driving (downward displacement from equilibrium). At 21.8 s, the top kinesin remains driving, while the bottom kinesin hinders the microtubule, causing the microtubule velocity to fall to 400 nm/s. At 35.0 s, the microtubule glides past the bottom kinesin, and the top kinesin becomes the sole driver, moving the microtubule at 800 nm/s.

MiCA Allows Purification of as Little as 30 ng DDB Bound to QD. The dynein-dynactin-BICD2N (DDB)
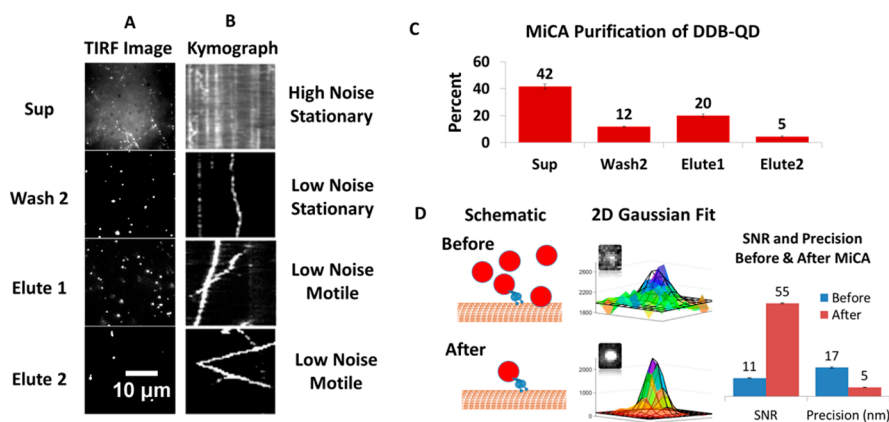
Figure 5. MiCA purification of DDB-QD. (A,B) TIRF images and kymographs of DDB-QD purification. The amount of DDB-QD left after binding to MiCA capture beads (Sup), left in second wash (Wash 2), and eluting through first and second elution (Elute 1 and 2) are shown in (A) and quantified in (C). Total yield including Elute 1 and 2 is 25%. Free QDs and unbound DDB-QDs contribute to high background noise in Sup. After 2 wash cycles, they are removed, shown by the low background noise in Wash 2, Elute 1, and Elute 2. (B) Kymographs showing DDB-QDs to be stationary or diffusive in Sup and Wash 2, but processive in Elute 1 and 2. This is also shown in Movie S2. Panel (D) compares the signal-to-noise (SNR) and precision obtained from QDs before MiCA (Sup) and after MiCA (Elute 1). High background before MiCA causes low SNR (5× less than after MiCA) and poor localization precision (∼3× worse than after MiCA). 7−16 frames are collected for yield quantification in panel (C). 1500−1800 QD frames are collected to quantify the SNR and precision in panel (D).

complex is difficult to isolate and its purification yield is typically much lower than that of kinesin. It has recently been of interest because binding of BICD2N allows dynein-dynactin to be ultraprocessive[46,47] and increases its force production 4-fold.[33] In our hands, DDB needs to be mixed with 5−10× more QD in molar ratio, in order to bind (nonspecifically) to QD. Our successful purification of DDB-QD with MiCA demonstrates that MiCA is able to purify a very small quantity of a traditionally challenging protein (30 ng), and that a large excess of QD (5−10×) can be removed with MiCA, significantly increasing the pool of active DDB-QD. Detailed protocol for MiCA purification of DDB-QD and its quantification using TIRF microscopy are laid out in Materials and Methods. Figure 5 shows the result of successful purification of DDB-QD. Optimization experiment for DDB-QD is described in Supporting Information section 13.

Figure 5A,B shows TIRF images and kymographs of DDB-QD purification. The amount of DDB-QD left after binding to MiCA capture beads (Sup), left in second wash (Wash 2), and eluting through first and second elution (Elute 1 and 2) are shown in (A) and quantified in (C). Total yield including Elute 1 and 2 is 25%. Free QDs and unbound DDB-QDs contribute to high background noise in Sup. After 2 wash cycles, they are removed, as shown by the low background noise in Wash 2, Elute 1, and Elute 2. Figure 5B shows kymographs of DDB-QDs, which are stationary or diffusive in Sup and Wash 2, but processive in Elute 1 and 2. This is also shown in Movie S2.

To quantify the extent to which excess QDs are removed, we look at the background created by the excess QD, which will reduce the signal-to-noise ratio (SNR) and worsen the spatial precision of DDB-QD after fitting a 2D Gaussian and analyzed using FIONA.[48] The SNR is the ratio between the peak and base of the 2D Gaussian fit, and the spatial precision calculation using FIONA takes into account the number of photons, finite pixel size, and background. Figure 5D compares the SNR and precision obtained from QDs before (Sup) and after MiCA (Elute 1). The SNR before MiCA (11) is 5× less than after MiCA (55). The spatial precision achieved before MiCA (17 nm) is ∼3× worse than after MiCA (5 nm).

Optimizing MiCA Purification. Discussions on the general strategy for MiCA purification and its limitations are outlined in Supporting Information sections 17 and 18.

■ CONCLUSIONS

MiCA purification is ideal for point-of-use purification of a molecular motor either by itself or attached to a cargo. It is fast and able to purify a small quantity of motors. In this paper, we have shown successful purification of kinesin, kinesin-QD, and DDB-QD with MiCA. The purification yield is as high as 27%, and it is able to purify as little as 30 ng DDB-QD. We also demonstrate a proof-of-principle of force-gliding assay, which allows parallel force detections from multiple kinesin-QDs for the first time. MiCA purification shortens purification time from 2 h to 20 min, lending itself to routine purification of conjugated motors for a wide range of single molecule and biomolecular experiments. It is expected to be widely useful, although one must be aware of the disruption of cytoskeleton binding to the PEG-amine magnetic bead due to high salt and casein. In addition, it may be possible to extend this procedure to cell extracts.

■ MATERIALS AND METHODS

Preparation of Kinesin. Three different types of kinesin are used. All of them are truncated kinesin with biotin attached either to the C-terminus where the cargo binding domain of full length kinesin lies, or the N-terminus where the catalytic domain lies. The shortest kinesin used is K432, a 432-amino-acid fraction of *Drosophila* kinesin. The next two kinesins, K888 and K888-Het, are equally long with 888 amino acids from the mouse kinesin heavy chain. K888 is a homodimer with biotin on the C terminus of both monomers, while K888-Het is a heterodimer with biotin on the N-terminus of only one of the two monomers. The preparation of all kinesin is detailed in Supporting Information section 11.

Preparation of Dynein-Dynactin-BICD2N (DDB) Complex. DDB was prepared from porcine brain lysate.[46,47] Briefly, fresh porcine brain was obtained from the slaughterhouse. It was then cut into small pieces and frozen into batch aliquots.

When needed, a fresh batch of lysate was prepared by thawing an aliquot at 37 °C and homogenizing in a 1:1 ratio with 50 mM Hepes, 50 mM Pipes pH 7.0, 1 mM EDTA, and 2 mM MgSO$_4$ in a Waring blender. The lysate was then transferred to a glass douncer and further homogenized with a Teflon pestle. This was followed by a 30 min spin at 30 000 × g. Lysates were flash frozen in 2 mL aliquots at this point. Prior to performing the DDB pull-down assay, aliquots were thawed and further clarified at 100 000 × g for 10 min before use. For purifying DDB, 500 μL of porcine brain lysate was mixed together with BICD2N[47] to a final concentration of 100 nM and 100 μL of a 50% Strep-tactin Sepharose bead slurry (GE Healthcare). NP-40, PMSF, and DTT was added to a final concentration of 0.1%, 1 mM, and 5 mM, respectively. The mixture was incubated while rotating for 1 h at 4 °C and then washed 4 times with Buffer A (30 mM Hepes, pH 7.4, 50 mM potassium acetate, 2 mM magnesium acetate, 1 mM EGTA, and 10% glycerol) containing 0.1% NP-40 and 5 mM DTT. The DDB complexes were then eluted by incubating the beads with 100 μL of Buffer A containing 2.5 mM of desthiobiotin. Sucrose was added to a final concentration of 6%, and the DDB were then flash frozen as aliquots.

Kinesin Purification with Microtubule Affinity and MiCA Purification Monitored Using Gel Electrophoresis. Long microtubules are prepared by polymerizing 8 μL tubulin (5 mg/mL) in 1 mM GMP-CPP for 30 min at 37 °C. 15 μL GMP-Taxol buffer (20 μM paclitaxel, 1 mM GMP-CPP in BRB80) is then added and the solution is divided into 2 tubes of 10 μL each. One tube is centrifuged for 30 min at 13 000 × g, and then reconstituted in 10 μL GMP-Taxol buffer to make the long microtubules. The other tube is sonicated for 3 min at room temperature to make the short microtubules. Any buffer coming into contact with microtubules should be warmed to room temperature.

MiCA capture bead is prepared by removing the buffer in 50 μL PEG-amine bead (10 mg/mL) and mixing in 6.25 μL short microtubules. The mixture is left to incubate for 5 min, and reconstituted in 5 μL dilution taxol buffer (20 μM paclitaxel, 1 mM THP, and 80 nM ATP in DmB−dynein motility buffer: 30 mM HEPES, 50 mM KAcetate, 2 mM MgAcetate, 1 mM EGTA, pH 7.2). 5 μL DmB-BSA is then added, and the mixture incubated for 2 min followed by washing with 10 μL dilution taxol buffer. Finally the beads are reconstituted in 5 μL dilution taxol buffer to make a final volume of ~6 μL.

K888-Het is diluted 4× to ~3.75 μM in dilution-taxol buffer. For traditional affinity purification, 1 μL of this diluted K888-Het is mixed with 3.5 μL long microtubules, 1 μL AMP-PNP (8 mM), and 2.5 μL dilution taxol buffer. For MiCA purification, 1 μL K888-Het (3.75 μM) is mixed with 6 μL MiCA capture bead and 1 μL AMP-PNP (8 mM). The mixtures are incubated for 5 min at room temperature in an end-to-end rotator.

The kinesin-microtubule and kinesin-bead are washed with 8 μL dilution taxol buffer twice. For traditional affinity purification, washing is done by centrifuging mixture at 13 000 × g for 30 min at room temperature to pellet the kinesin-microtubule, and then gently add and remove dilution taxol buffer without disturbing the pellet. For MiCA purification, washing is done by magnetic separation to pellet the kinesin-bead, then the buffer is removed and the pellet reconstituted in dilution taxol buffer.

Once washed, the pellets are reconstituted in 8 μL elution buffer (3 mM ATP in dilution taxol buffer) and left to incubate

for 5 min. The eluants are collected through centrifugation or magnetic separation, and another 8 μL elution buffer is added and incubated for 5 min. The second batches of eluants are again collected.

The AMP-PNP supernatant, two wash batches, two elution batches, and proteins left in bead or pellet are then quantified with SDS-PAGE electrophoresis using Imperial protein stain (Cat. 24615, ThermoFisher Scientific).

Microtubule Gliding Assay with Kinesin-QD after MiCA Purification. Kinesin-QD is prepared by mixing 0.2 μL K888 (8.8 μM, or 640 ng with molecular weight of 360 kDa per kinesin dimer), 1 μL Qdot 655 Streptavidin Conjugate (SA-Qd655, 1 μM), and 1.8 μL BSA-taxol buffer (20 μM paclitaxel, 1 mM THP, and 80 nM ATP in DmB-BSA) and incubated for at least 5 min on ice. 2 μL short microtubules are thawed from a frozen aliquot of short microtubules prepared as described. MiCA capture bead is prepared by mixing 2 μL short microtubules with 8 μL PEG-amine bead pellet (10 mg/mL) with its buffer removed. After 5 min incubation, the MiCA capture bead is washed 2× with 8 μL BSA-taxol buffer and reconstituted in 2 μL BSA-taxol buffer to give 3 μL final bead volume. Next, 4 μL kinesin-QD is mixed with 3 μL MiCA capture bead and 1 μL AMP-PNP (8 mM), and then incubated for 5 min at room temperature. The mixture is then washed twice with 8 μL BSA-taxol buffer and 8 μL elution buffer (3 mM ATP in BSA-taxol buffer) is added. After 5 min incubation, the eluant is extracted that yields approximately 100 nM kinesin-QD.

For the gliding assay, long fluorescent microtubules are prepared as in Supporting Information section 5, using HyLite 488 as the fluorescent tubulin. Approximately 0.2 nM kinesin-QD before and after MiCA purification is added to biotin-PEG chamber and left to incubate for 5 min. The chamber is then washed with four chamber volume of BSA-taxol buffer, and imaging buffer containing 1 mM ATP, 10× dilution long microtubules, 1 mM THP, 20 μM paclitaxel, 50 μM biotin, 10 U/mL pyranose oxidase, 4000 U/mL catalase, and 2% glucose is added. The chamber is then imaged on TIRF microscope with exposure time of 2 s on two EMCCD camera, one to collect the QD fluorescence, another to collect the microtubule fluorescence. A set of nanohole images on both cameras are also collected for image registration.

For analysis, a transform function is obtained with the nanohole images, as shown in Supporting Figure S7. The QD images are then transformed so that they are registered with the microtubule images. The microtubule image is binarized, thinned to single pixel, and then dilated to give it some width. The location of each QD is found using TrackMate in ImageJ. Binary locations of the QDs are then overlaid with binary microtubule images, and QD points that overlap with microtubules for at least 8 frames are considered active.

Force-Gliding Assay. MiCA purification of kinesin-QD, BSA taxol buffer, long fluorescent microtubules, imaging buffer, and image registration is performed the same way as the microtubule gliding assay experiment. Kinesin-QD (2 μL, 80 nM) is mixed with Dig-DNA-Biotin (0.25 μL, 80 nM, 1565 base-pair DNA prepared by PCR of pBR322 plasmid with forward primer conjugated to biotin and reverse primer conjugated to dig). Forward primer sequence is/5BiosG/AC AGC ATC GCC AGT CAC TAT G and reverse primer sequence is/5DiGN/GG GAC CAG AGA AAA ATC ACT CAG G. Both are purchased from IDT-DNA using HPLC for purification. There is ~8× less DNA than kinesin-QD to

ensure that kinesin-QD has at most 1 DNA attached. After 10 min incubation, 0.2 μL biotin (10 mM) is added to the kinesin-QD-DNA mixture.

To prepare flow chamber, 600 nM Streptavidin is added to fill a biotin-PEG chamber (∼1.5 μL volume) and incubated for >5 min. The chamber is then washed with 10 μL DmB-BSA, and then 1.5 μL anti-Dig-biotin (10 nM) is added and incubated for >5 min. The chamber is then washed with 5 μL DmB-BSA supplemented with 250 μM biotin to saturate the streptavidin surface with biotin. 2 μL kinesin-QD-DNA (adjusted to 0.1 nM DNA concentration) is then added to the chamber and incubated for >5 min. The chamber is then washed with 6 μL BSA-Taxol buffer with 250 μM biotin. Imaging buffer containing long fluorescence microtubules, ATP, and oxygen scavenging reagents is then added and the chamber is imaged in a TIRF microscope with green laser and 0.2 s exposure time and 1500 frames.

MiCA Purification of DDB-QD. 3 μL DDB (∼20 nM or ∼30 ng/μL dynein) is mixed with 3 μL SA-Qd705 (100 nM) and incubated for >3 h on ice. 2 μL frozen short microtubules are thawed and warmed with hands, and then mixed with 8 μL PEG-amine beads which has its buffer removed after magnetic pull. The mixture is incubated for 5 min at room temperature, then washed 2× with BSA-taxol buffer. On final wash, 7 μL BSA-taxol buffer is added to make 8 μL final solution. This bead solution is then aliquoted into 3 tubes in increasing volume: 0.4, 1.6, and 6 μL, which are labeled as 1×, 4×, and 15× beads. The buffers of these aliquots are then removed and 1 μL BSA-taxol is added to each. Next, 2 μL DDB-QD is added to each bead sample, and the mixtures are left to incubate at room temperature for 10 min on an end-to-end rotator. The 3 μL supernatant is then removed and labeled "Bind". The pellet is washed twice with 3 μL BSA-taxol, labeled "Wash 1" and "Wash 2". The final pellet is eluted twice with 3 μL elution buffer (1 mM ATP in BSA-taxol) and 5 min incubation. These are "Elute 1" and "Elute 2".

The Bind, Wash 1, and Wash 2 samples are then mixed with 0.25 μL biotin (10 mM) to saturate all streptavidin binding sites on QD, then flowed into microtubule chambers made from PEG-biotin slide layered with streptavidin and long biotin-fluorescent microtubules. DDB-QDs in these samples will bind to microtubules on the chamber. Elute 1 and Elute 2 are diluted twice in imaging buffer, yielding final solution with 0.6 mM ATP, 1 mM THP, 20 μM paclitaxel, 50 μM biotin, 10 U/mL pyranose oxidase, 4000 U/mL catalase, and 2% glucose in DmB-BSA. These final solutions are then flowed into the microtubule chamber. All images are recorded on TIRF microscope after ∼5 min from infusion into the microtubule chamber. Particle counting is done with TrackMate in ImageJ. Signal to noise ratios (SNR) and precision values are obtained by fitting 2d Gaussians to 16 dots from each Bind and Elute 1 movie. This is done using in-house program in Matlab. Each dot consists of 22 to 200 frames that are 0.5s apart in time. The amplitudes and background noises from the Gaussian fits and raw images are used to compute the SNR and precision values.

■ ASSOCIATED CONTENT

Ⓢ Supporting Information

The Supporting Information is available free of charge on the ACS Publications website at DOI: 10.1021/acs.bioconjchem.8b00264.

Microtubule gliding experiments using kinesin-QD before and after MiCA purification (AVI)

Kymographs as in Figure 5 (AVI)

Kinesin-QD moves well on microtubules adhered to the PEG-amine surface (AVI)

Force-gliding assay (AVI)

Kymographs as in Figure S8 (AVI)

Preparation of short microtubules; Microtubule affinity purification; Magnetic beads preparation; Effect of BSA blocking on amine and PEG-amine beads; Preparation of long fluorescent microtubules; Experiments on amine and PEG-amine coverslips; Preparation of PEG-biotin coverslips; Effect of sonication and freeze-thawing on microtubule length; Binding and release of kinesin-QD to tubulin and various microtubule preparations; Effect of freeze-thawing microtubules on kinesin elution; Preparation of kinesin; Image registration; DDB-QD and MiCA purification optimization; Microtubule release with casein, KCl and ATP; Accuracy of force measurements with force-gliding assay; General strategy for MiCA optimization; Limitations of MiCA purification (PDF)

■ AUTHOR INFORMATION

Corresponding Author

*E-mail: selvin@illinois.edu.

ORCID Ⓘ

Marco Tjioe: 0000-0002-6445-9828

Yuji Ishitsuka: 0000-0002-6780-7154

Kathleen M. Trybus: 0000-0002-5583-8500

Notes

The authors declare no competing financial interest.

■ REFERENCES

(1) Veigel, C., and Schmidt, C. F. (2011) Moving into the Cell: Single-Molecule Studies of Molecular Motors in Complex Environments. *Nat. Rev. Mol. Cell Biol.* 12 (3), 163−176.

(2) Hirokawa, N., and Takemura, R. (2003) Biochemical and Molecular Characterization of Diseases Linked to Motor Proteins. *Trends Biochem. Sci.* 28 (10), 558−565.

(3) De Vos, K. J., Grierson, A. J., Ackerley, S., and Miller, C. C. J. (2008) Role of Axonal Transport in Neurodegenerative Diseases. *Annu. Rev. Neurosci.* 31 (1), 151−173.

(4) Stokin, G. B., and Goldstein, L. S. B. (2006) Linking Molecular Motors to Alzheimer's Disease. *J. Physiol.* 99 (2), 193−200.

(5) Kumar, K. R. S., Kamei, T., Fukaminato, T., and Tamaoki, N. (2014) Complete ON/OFF Photoswitching of the Motility of a Nanobiomolecular Machine. *ACS Nano* 8 (5), 4157−4165.

(6) Hiratsuka, Y., Tada, T., Oiwa, K., Kanayama, T., and Uyeda, T. Q. P. (2001) Controlling the Direction of Kinesin-Driven Microtubule Movements along Microlithographic Tracks. *Biophys. J.* 81 (3), 1555−1561.

(7) van den Heuvel, M. G. L., and Dekker, C. (2007) Motor Proteins at Work for Nanotechnology. *Science* 317 (5836), 333−336.

(8) Bakewell, D. J. G., and Nicolau, D. V. (2007) Protein Linear Molecular Motor-Powered Nanodevices. *Aust. J. Chem.* 60 (5), 314−332.

(9) Agarwal, A., and Hess, H. (2010) Biomolecular Motors at the Intersection of Nanotechnology and Polymer Science. *Prog. Polym. Sci.* 35 (1), 252−277.

(10) Aoyama, S., Shimoike, M., and Hiratsuka, Y. (2013) Self-Organized Optical Device Driven by Motor Proteins. *Proc. Natl. Acad. Sci. U. S. A.* 110 (41), 16408−16413.

(11) Fujimoto, K., Kitamura, M., Yokokawa, M., Kanno, I., Kotera, H., and Yokokawa, R. (2013) Colocalization of Quantum Dots by Reactive Molecules Carried by Motor Proteins on Polarized Microtubule Arrays. *ACS Nano* 7 (1), 447−455.

(12) Finer, J. T., Simmons, R. M., and Spudich, J. A. (1994) Single Myosin Molecule Mechanics: Piconewton Forces and Nanometre Steps. *Nature* 368 (6467), 113−119.

(13) Yildiz, A., Forkey, J. N., McKinney, S. A., Ha, T., Goldman, Y. E., and Selvin, P. R. (2003) Myosin V Walks Hand-Over-Hand: Single Fluorophore Imaging with 1.5-Nm Localization. *Science* 300 (5628), 2061−2065.

(14) Yildiz, A., Tomishige, M., Vale, R. D., and Selvin, P. R. (2004) Kinesin Walks Hand-Over-Hand. *Science* 303 (5658), 676−678.

(15) Molloy, J. E., Burns, J. E., Kendrick-Jones, J., Tregear, R. T., and White, D. C. S. (1995) Movement and Force Produced by a Single Myosin Head. *Nature* 378 (6553), 209−212.

(16) Svoboda, K., Schmidt, C. F., Schnapp, B. J., and Block, S. M. (1993) Direct Observation of Kinesin Stepping by Optical Trapping Interferometry. *Nature* 365 (6448), 721−727.

(17) Block, S. M. (2007) Kinesin Motor Mechanics: Binding, Stepping, Tracking, Gating, and Limping. *Biophys. J.* 92 (9), 2986−2995.

(18) Gennerich, A., and Vale, R. D. (2009) Walking the Walk: How Kinesin and Dynein Coordinate Their Steps. *Curr. Opin. Cell Biol.* 21 (1), 59−67.

(19) Sellers, J. R., and Veigel, C. (2006) Walking with Myosin V. *Curr. Opin. Cell Biol.* 18 (1), 68−73.

(20) Kural, C., Kim, H., Syed, S., Goshima, G., Gelfand, V. I., and Selvin, P. R. (2005) Kinesin and Dynein Move a Peroxisome in Vivo: A Tug-of-War or Coordinated Movement? *Science* 308 (5727), 1469−1472.

(21) Mehta, A. D., Rock, R. S., Rief, M., Spudich, J. A., Mooseker, M. S., and Cheney, R. E. (1999) Myosin-V Is a Processive Actin-Based Motor. *Nature* 400 (6744), 590−593.

(22) Altman, D., Sweeney, H. L., and Spudich, J. A. (2004) The Mechanism of Myosin VI Translocation and Its Load-Induced Anchoring. *Cell* 116 (5), 737−749.

(23) Gennerich, A., Carter, A. P., Reck-Peterson, S. L., and Vale, R. D. (2007) Force-Induced Bidirectional Stepping of Cytoplasmic Dynein. *Cell* 131 (5), 952−965.

(24) Svoboda, K., and Block, S. M. (1994) Force and Velocity Measured for Single Kinesin Molecules. *Cell* 77 (5), 773−784.

(25) Veigel, C., Wang, F., Bartoo, M. L., Sellers, J. R., and Molloy, J. E. (2002) The Gated Gait of the Processive Molecular Motor, Myosin V. *Nat. Cell Biol.* 4 (1), 59−65.

(26) Nelson, S. R., Ali, M. Y., and Warshaw, D. M. (2011) Quantum Dot Labeling Strategies to Characterize Single-Molecular Motors. In *Single Molecule Enzymology*, Methods in Molecular Biology, pp 111−121, Humana Press.

(27) Muthukrishnan, G., Hutchins, B. M., Williams, M. E., and Hancock, W. O. (2006) Transport of Semiconductor Nanocrystals by Kinesin Molecular Motors. *Small* 2 (5), 626−630.

(28) Seitz, A., and Surrey, T. (2006) Processive Movement of Single Kinesins on Crowded Microtubules Visualized Using Quantum Dots. *EMBO J.* 25 (2), 267−277.

(29) Schneider, R., Korten, T., Walter, W. J., and Diez, S. (2015) Kinesin-1 Motors Can Circumvent Permanent Roadblocks by Side-Shifting to Neighboring Protofilaments. *Biophys. J.* 108 (9), 2249−2257.

(30) Ori-McKenney, K. M., Xu, J., Gross, S. P., and Vallee, R. B. (2010) A Cytoplasmic Dynein Tail Mutation Impairs Motor Processivity. *Nat. Cell Biol.* 12 (12), 1228−1234.

(31) Toba, S., Watanabe, T. M., Yamaguchi-Okimoto, L., Toyoshima, Y. Y., and Higuchi, H. (2006) Overlapping Hand-over-Hand Mechanism of Single Molecular Motility of Cytoplasmic Dynein. *Proc. Natl. Acad. Sci. U. S. A.* 103 (15), 5741−5745.

(32) DeWitt, M. A., Chang, A. Y., Combs, P. A., and Yildiz, A. (2012) Cytoplasmic Dynein Moves Through Uncoordinated Stepping of the AAA+ Ring Domains. *Science* 335 (6065), 221−225.

(33) Belyy, V., Schlager, M. A., Foster, H., Reimer, A. E., Carter, A. P., and Yildiz, A. (2016) The Mammalian Dynein-Dynactin Complex Is a Strong Opponent to Kinesin in a Tug-of-War Competition. *Nat. Cell Biol.* 18 (9), 1018−1024.

(34) Vale, R. D., Reese, T. S., and Sheetz, M. P. (1985) Identification of a Novel Force-Generating Protein, Kinesin, Involved in Microtubule-Based Motility. *Cell* 42 (1), 39−50.

(35) Derr, N. D., Goodman, B. S., Jungmann, R., Leschziner, A. E., Shih, W. M., and Reck-Peterson, S. L. (2012) Tug-of-War in Motor Protein Ensembles Revealed with a Programmable DNA Origami Scaffold. *Science* 338 (6107), 662−665.

(36) Belyy, V., Hendel, N. L., Chien, A., and Yildiz, A. (2014) Cytoplasmic Dynein Transports Cargos via Load-Sharing between the Heads. *Nat. Commun.* 5, 5544.

(37) Verbrugge, S., Kapitein, L. C., and Peterman, E. J. G. (2007) Kinesin Moving through the Spotlight: Single-Motor Fluorescence Microscopy with Submillisecond Time Resolution. *Biophys. J.* 92 (7), 2536−2545.

(38) Reck-Peterson, S. L., Yildiz, A., Carter, A. P., Gennerich, A., Zhang, N., and Vale, R. D. (2006) Single-Molecule Analysis of Dynein Processivity and Stepping Behavior. *Cell* 126 (2), 335−348.

(39) Yildiz, A., Tomishige, M., Gennerich, A., and Vale, R. D. (2008) Intramolecular Strain Coordinates Kinesin Stepping Behavior along Microtubules. *Cell* 134 (6), 1030−1041.

(40) Sikora, A., Canova, F. F., Kim, K., Nakazawa, H., Umetsu, M., Kumagai, I., Adschiri, T., Hwang, W., and Teizer, W. (2015) Behavior of Kinesin Driven Quantum Dots Trapped in a Microtubule Loop. *ACS Nano* 9 (11), 11003−11013.

(41) Warshaw, D. M., Kennedy, G. G., Work, S. S., Krementsova, E. B., Beck, S., and Trybus, K. M. (2005) Differential Labeling of Myosin V Heads with Quantum Dots Allows Direct Visualization of Hand-Over-Hand Processivity. *Biophys. J.* 88 (5), L30−L32.

(42) Berensmeier, S. (2006) Magnetic Particles for the Separation and Purification of Nucleic Acids. *Appl. Microbiol. Biotechnol.* 73 (3), 495−504.

(43) Safarik, I., and Safarikova, M. (2004) Magnetic Techniques for the Isolation and Purification of Proteins and Peptides. *Biomagn. Res. Technol.* 2, 7.

(44) Fields, G. (1995) Methods for Removing the Fmoc Group. In *Peptide Synthesis Protocols*, Methods in Molecular Biology (Pennington, M., and Dunn, B., Eds.) pp 17−27, Humana Press.

(45) Grover, R., Fischer, J., Schwarz, F. W., Walter, W. J., Schwille, P., and Diez, S. (2016) Transport Efficiency of Membrane-Anchored Kinesin-1 Motors Depends on Motor Density and Diffusivity. *Proc. Natl. Acad. Sci. U. S. A.* 113 (46), E7185−E7193.

(46) McKenney, R. J., Huynh, W., Tanenbaum, M. E., Bhabha, G., and Vale, R. D. (2014) Activation of Cytoplasmic Dynein Motility by Dynactin-Cargo Adapter Complexes. *Science* 345 (6194), 337−341.

(47) Huynh, W., and Vale, R. D. (2017) Disease-Associated Mutations in Human BICD2 Hyperactivate Motility of Dynein−Dynactin. *J. Cell Biol.* 216 (10), 3051−3060.

(48) Selvin, P. R., Lougheed, T., Hoffman, M. T., Park, H., Balci, H., Blehm, B. H., and Toprak, E. (2007) Fluorescence Imaging with One-Nanometer Accuracy (FIONA). *Cold Spring Harb. Protoc.* 2007 (10), pdb.top27.